Mechanism of High-Temperature Superconductivity in Correlated-Electron Systems

Takashi Yanagisawa

National Institute of Advanced Industrial Science and Technology 1-1-1 Umezono, Tsukuba, Ibaraki 305-8568, Japan; t-yanagisawa@aist.go.jp

Abstract: It is very important to elucidate the mechanism of superconductivity for achieving room temperature superconductivity. In the first half of this paper, we give a brief review on mechanisms of superconductivity in many-electron systems. We believe that high-temperature superconductivity may occur in a system with interaction of large-energy scale. Empirically, this is true for superconductors that have been found so far. In the second half of this paper, we discuss cuprate high-temperature superconductors. We argue that superconductivity of high temperature cuprates is induced by the strong on-site Coulomb interaction, that is, the origin of high-temperature superconductivity is the strong electron correlation. We show the results on the ground state of electronic models for high temperature cuprates on the basis of the optimization variational Monte Carlo method. A high-temperature superconducting phase will exist in the strongly correlated region.

Keywords: strongly correlated electron systems; mechanisms of superconductivity; high-temperature superconductivity; kinetic driven superconductivity; optimization variational Monte Carlo method; Hubbard model; three-band d-p model

1. Introduction

It is a challenging research subject to clarify the mechanism of high temperature superconductivity, and indeed it has been studied intensively for more than 30 years [1–3]. For this purpose, it is important to clarify the ground state and phase diagram of electronic models with strong correlation because high temperature cuprates are strongly correlated electron systems.

Most superconductors induced by the electron–phonon interaction have *s*-wave pairing symmetry. We can understand physical properties of *s*-wave superconductivity based on the Bardeen–Cooper–Schrieffer (BCS) theory [4–6]. The critical temperature T_c of most of electron–phonon superconductors is very low except for exceptional compounds. Many unconventional superconductors that cannot be understood by the BCS theory have been discovered. They are, for example, heavy fermion superconductors, organic superconductors and cuprate superconductors for which the pairing mechanism is different from the electron–phonon interaction. In particular, cuprate superconductors exhibit relatively high T_c and have become of great interest. A common feature in both electron–phonon systems and correlated electron systems is that critical temperature may have a strong correlation with the energy scale of the interaction that induces electron pairing.

This paper has two parts. In the first part, we give a review on mechanisms of superconductivity in the electron–phonon system and in the correlated electron system. In the second part, we mainly discuss the mechanism of high-temperature cuprates.

The model for CuO_2 plane in cuprate superconductors is called the d-p model or the three-band Hubbard model [7–24]. It is certainly a very difficult task to elucidate the phase diagram of the d-p model. Simplified models are also used to investigate the mechanism of superconductivity, for example the two-dimensional (2D) single-band Hubbard model [25–50] and ladder model [51–56].

The Hubbard model was introduced to understand the metal–insulator transition [57] and was employed to understand various magnetic phenomena [58,59]. On the basis of the Hubbard model, it is possible to understand the appearance of inhomogeneous states reported for cuprates, such as stripes [60–67] and checkerboard-like density wave states [68–71]. It was also expected that the Hubbard model can account for high temperature superconductivity [72].

A variational Monte Carlo method is used to examine the ground state properties of strongly correlated electron systems, where we calculate the expectation values exactly using a numerical method [28–31,36–41]. We introduced the wave function of $\exp(-S)$-type in the study of superconductivity in the Hubbard model [73–75]. This wave function is very excellent in the sense that the energy expectation value is lower than that of any other wave functions [50].

The paper is organized as follows. In Section 2.1, we discuss the phonon mechanism of superconductivity. In Section 2.2, we discuss the electron mechanism of superconductivity. Section 2.3 is devoted to a discussion on superconductivity in correlated electron systems. In Section 3.1, we show the model for high temperature cuprates. We present the optimization variational Monte Carlo method (OVMC) in Section 3.2. We show the results on superconductivity based on the OVMC in Section 3.3. We discuss the stability of antiferromagnetic state in Section 3.4. We show the phase diagram when the hole doping rate is changed in Section 3.5. We give a summary in Section 4.

2. Part I. Superconductivity in Many-Electron Systems

2.1. Possibility of High-T_c Superconductivity

In the BCS theory, the electron–phonon interaction is assumed to induce attractive interaction between electrons and the pairing symmetry is *s*-wave [4–6]. There are many superconductors with *s*-wave pairing symmetry and most of them are due to the electron–phonon interaction. The BCS theory was successful to explain physical properties of these superconductors.

In the strong-coupling theory based on the Green function formulation [76,77], the critical temperature T_c was estimated as [78],

$$T_c = \frac{\theta_D}{1.45} \exp\left(-\frac{1.04(1+\lambda)}{\lambda - \mu^*(1 + 0.62\lambda)}\right),$$ (1)

where λ is the electron–phonon coupling constant, $\theta_D = \hbar\omega_D/k_B$ is the Debye temperature and μ^* is the renormalized Coulomb parameter defined by

$$\mu^* = \frac{\mu}{1 + \mu\ln(\epsilon_F/\omega_D)},$$ (2)

for $\mu = U/\epsilon_F$ where U is the strength of the Coulomb interaction and ϵ_F is the Fermi energy. μ^* is the phenomenological parameter being approximately 0.1.

The electron–phonon coupling constant λ is expressed as

$$\lambda = 2\int_0^\infty d\omega \frac{\alpha(\omega)^2 F(\omega)}{\omega},$$ (3)

where $\alpha(\omega)$ is the averaged electron–phonon coupling over the Fermi surface and $F(\omega)$ indicates the product of the spectral function of phonon and the density of states. This is approximately written as

$$\lambda \simeq \frac{\rho(\epsilon_F)\langle I\rangle^2}{M\omega_D^2},$$ (4)

where $\rho(\epsilon_F)$ is the density of states at the Fermi surface and M is the mass of an atom. McMillan predicted that T_c would have a limit being of the order of 30 K from the analysis for this formula [78].

The McMillan formula was modified by replacing $\theta_D/1.45$ by logarithmic Debye frequency $\omega_{\ln}$ where [79]

$$\omega_{\ln} = \exp\left(\frac{2}{\lambda}\int_0^\infty d\omega \alpha(\omega)^2 F(\omega)\frac{\ln\omega}{\omega}\right). \tag{5}$$

It was predicted that high critical temperature would be possible for large λ since $T_c \propto \sqrt{\lambda}$ for $\lambda \gg 1$. If $\omega_{\ln}$ is large, λ is also large, and the crystal is stable, high T_c would be realized. It was predicted that high T_c would be realized in hydrogen solid with high Debye temperature [80]. In fact, high temperature superconductors with T_c above 200 K were discovered under extremely high pressure (160∼200 GPa) in hydrogen compounds such as H_3S and LaH_{10} [81–83].

It is important to consider multi-band superconductors in the search for high temperature superconductors. In fact, MgB_2 and iron based superconductors are multi-band superconductors. An important role of Lifshitz transition in iron based superconductors and MgB_2 multi-band superconductors has been predicted [84]. An interesting point is that the possibility of high-T_c superconductivity in materials where tuning the chemical potential shows a quasi-1D Fermi surface topology as in organics and hydrides [85]. A layered superconductor such as cuprate superconductor can be regarded as a multiband superconductor due to interlayer couplings. A multi-band superconductivity has been investigated as a generalization of the BCS theory since early works on the two-band superconductivity [86–89]. There will appear many interesting properties in superconductors with multiple gaps such as time-reversal symmetry breaking [90–103], the existence of massless modes [104–109], unusual isotope effect [110–114] and fractional-flux quantum vortices [115–119]. When we have multiple order parameters, there appear multiple Nambu–Goldstone bosons and Higgs bosons [104,120–129]. This will result in significant excitation modes that are unique in multi-band superconductors.

It is important to include in a theoretical picture the presence of multiple electronic components with anomalous normal state properties in the charge and spin sector, e.g., the well known Fermi arcs and charge pseudogap phenomenology. The "shape resonance" scenario of multigap BCS-BEC crossover has been proposed [130,131]. The study of the electronic structure of the cuprates superconductors $Bi_2Sr_2CaCuO_{8+y}$ and La_2CuO_{4+y} doped by mobile oxygen interstitials using local probes has shown a scenario made of two electronic components: a strongly correlated Fermi liquid which coexists with stripes made of anisotropic polarons condensed into a generalized Wigner charge density wave [132–134].

2.2. Electron Correlation and Superconductivity

We discuss the electron correlation due to the Coulomb interaction between electrons. The on-site Coulomb interaction is important in the study of the metal insulator transition and magnetic properties of materials. The Hubbard model is written as [25]

$$H = \sum_{ij\sigma} t_{ij} c_{i\sigma}^\dagger c_{j\sigma} + U\sum_i n_{i\uparrow}n_{i\downarrow}, \tag{6}$$

where t_{ij} indicates the transfer integral and the second term denotes the Coulomb interaction with the strength U. t_{ij} are chosen as follows. $t_{ij} = -t$ when i and j are nearest-neighbor pairs $\langle ij\rangle$ and $t_{ij} = -t'$ when i and j are next-nearest neighbor pairs. In the following, N is the number of lattices, and N_e denotes the number of electrons.

When two electrons spin up and down at the same site, the energy becomes higher by U where U denotes the on-site Coulomb energy. In the case of half-filling, the Mott transition occurs when $U(>0)$ is as large as the bandwidth and the ground state is an insulator. The effective Hamiltonian is derived

in the limit of large U/t [135–137], based on the canonical transformation $H_{\text{eff}} = e^{iS} H e^{-iS}$. In the limit $U/t \to \infty$, the double occupancy is not allowed. The effective Hamiltonian is written as

$$H_{\text{eff}} = H + i[S, H] + \frac{i^2}{2}[S, [S, H]] + \cdots. \tag{7}$$

We write the Hamiltonian as $H = \tilde{H}_0 + H_1$ where

$$\tilde{H}_0 = \sum_{ij\sigma} t_{ij}(a_{i\sigma}^\dagger a_{j\sigma} + d_{i\sigma}^\dagger d_{j\sigma}) + U \sum_i n_{i\uparrow} n_{i\downarrow}, \tag{8}$$

$$H_1 = \sum_{ij\sigma} t_{ij}(a_{i\sigma}^\dagger d_{j\sigma} + d_{j\sigma}^\dagger a_{i\sigma}). \tag{9}$$

Here, we defined $a_{i\sigma} = c_{i\sigma}(1 - n_{i,-\sigma})$ and $d_{i\sigma} = c_{i\sigma} n_{i,-\sigma}$. $a_{i\sigma} = c_{i\sigma}(1 - n_{i.-\sigma})$ is the electron operator without double occupancy. We choose S to satisfy $i[S, \tilde{H}_0] + H_1 = 0$, so that H_{eff} reads in the subspace of no double occupancy,

$$H_{\text{eff}} = \sum_{ij\sigma} t_{ij} a_{i\sigma}^\dagger a_{j\sigma} + \frac{i}{2}[S, H_1] + \frac{i^2}{3}[S, [S, H_1]] + \cdots. \tag{10}$$

When we consider only the nearest-neighbor transfer $t_{ij} = -t$, the effective Hamiltonian reads

$$\begin{aligned}
H_{\text{eff}} = & -t \sum_{\langle ij \rangle \sigma} a_{i\sigma}^\dagger a_{j\sigma} - \frac{t^2}{U} \sum_{j\mu\mu'} [a_{j+\mu\uparrow}^\dagger a_{j\downarrow}^\dagger a_{j\downarrow} a_{j+\mu'\uparrow} \\
& + a_{j\uparrow}^\dagger a_{j+\mu\downarrow}^\dagger a_{j+\mu'\downarrow} a_{j\uparrow} + a_{j+\mu\uparrow}^\dagger a_{j\downarrow}^\dagger a_{j+\mu'\downarrow} a_{j\uparrow} + a_{j\uparrow}^\dagger a_{j+\mu\downarrow}^\dagger a_{j\downarrow} a_{j+\mu\uparrow}],
\end{aligned} \tag{11}$$

where $j + \mu$ and $j + \mu'$ denote the nearest-neighbor sites in the μ and μ' directions, respectively. The second term being proportional to t^2/U contains the nearest-neighbor exchange interaction and also three-site terms when $\mu \neq \mu'$. The three-site terms are of the same order as the exchange interaction. When we neglect the three-site terms, the effective Hamiltonian reduces to the t-J model given by

$$H_{\text{eff}} = - \sum_{\langle ij \rangle \sigma} (a_{i\sigma}^\dagger a_{j\sigma} + \text{h.c.}) + J \sum_{\langle ij \rangle} \left(\mathbf{S}_i \cdot \mathbf{S}_j - \frac{1}{4} \tilde{n}_i \tilde{n}_j \right), \tag{12}$$

where $J = 4t^2/U$ and $\tilde{n}_i = \tilde{n}_{i\uparrow} + \tilde{n}_{i\downarrow}$ with $\tilde{n}_{i\sigma} = a_{i\sigma}^\dagger a_{i\sigma}$.

High-temperature cuprates and heavy fermion systems are typical correlated electron systems and many superconductors have been reported. Most of superconductors in these systems have nodes in the superconducting gap, namely, the Cooper pair is anisotropic. This indicates that superconductivity is unconventional and does not conform to the conventional BCS theory. The mechanism of superconductivity is certainly non-phonon mechanism. We show several characteristic properties of cuprate high-temperature superconductors:

1. The Cooper pair has *d*-wave symmetry.
2. The superconducting phase exists near the antiferromagnetic phase and parent materials are a Mott insulator.
3. The CuO_2 plane is commonly contained and the on-site Coulomb repulsive interaction works between *d* electrons.
4. The size of Cooper pair is very small being of order of 2 Å.
5. The CuO_2 plane is high anisotropic and there is a weak Josephson coupling between two layers.

The small size of Cooper pair also supports the non-phonon mechanism of cuprate superconductivity [138–141]. A plausible non-phonon mechanism is due to the Coulomb interaction on the same atom. Because the energy scale of the Coulomb interaction is very large, which is of

the order of eV, we can expect superconductivity with high critical temperature T_c. The critical temperature of heavy fermion materials is, however, very low, although superconductivity occurs due to strong Coulomb interaction between f electrons. This is because the effective mass of f electrons is very large in heavy fermion systems owing to the large self-energy correction. The effective mass enhancement of heavy fermion materials becomes as large as 100–1000, which means that the effective cutoff becomes very small. As a result, the characteristic energy scale is reduced considerably and the critical temperature T_c becomes very low begin of the order of 1 K. In heavy fermion systems, the characteristic energy scale is given by the Kondo temperature T_K. The ratio of the effective mass m^* to the band mass m_0 is approximately given as $m^*/m_0 \simeq D/T_K$ for the bandwidth D and T_K. Thus, the effective bandwidth for heavy fermions is given by the Kondo temperature $T_K \simeq D/(m^*/m_0)$. Empirically, T_c is lowered as the effective mass increases. This is expressed as follows:

$$k_B T_c \simeq 0.1t/(m^*/m_0), \tag{13}$$

where t denotes the transfer integral proportional to the bandwidth. The estimated values of the transfer t, the ratio m^*/m_0 and T_c for several compounds are shown in Table 1. For cuprates, the transfer t is estimated as $t \sim 0.51$ eV. The bandwidth for iron pnictides is about five times smaller than that for cuprates. A list of typical superconductors in correlated electron systems is shown in Table 2.

Table 1. The transfer integral t, effective mass m^* and critical temperature T_c in correlated electron systems, where m_0 denotes the band mass. The orders of these quantities are shown in the table. For heavy fermions, $t/(m^*/m_0)$ corresponds to the Kondo temperature T_K. For Hydrides, the Debye frequency $\omega_{\ln}$ is shown.

	t or $\omega_{\ln}$	m^*/m_0	$t/(m^*/m_0)$	T_c	
Cuprate superconductors	5000 K	5	1000	100 K	$t \sim 0.51$ eV [142]
Iron pnictides	1000 K	~ 2	500	50 K	$t \sim 0.1$ eV [143]
Heavy fermion materials	10,000 K	100~1000	10~100	1~10 K	[144–146]
Organic superconductors	200~500 K	2~5	100	10 K	[147]
Hydrides H_3S	1000 K	~ 1	1000	100 K	$\omega_{\ln}$ [148]

Table 2. Superconducting materials.

Materials	T_c	Pair Symmetry	Crystal Structure	
$CeCu_2Si_2$	0.6 K	s or d	bc tetragonal	[149,150]
UPt_3	0.52 K	p or f	Hexagonal	[151]
UBe_{13}	0.86 K	p	Cubic	[152]
URu_2Si_2	1.2 K		bc tetragonal	[153–155]
$CeRu_2$	6.2 K	s	Laves Cubic	[156]
UPd_2Al_3	2 K	d	Hexagonal	[157–159]
UNi_2Al_3	1 K	p?	Hexagonal	[158,160]
$CeCoIn_5$	2.3 K	d	$HoCoGa_5$ type	[161,162]
$CeRhIn_5$	2.1 K (16.3 kbar)	d	$HoCoGa_5$ type bc tetragonal	[163]
$CeRh_2Si_2$	0.35 K (9 kbar)		bc tetragonal	[164]
UGe_2	0.8 K (13.5 kbar)	p?	Orthorhombic	[165]
URhGe	0.25 K	p?	Orthorhombic	[166]
Sr_2RuO_4	1.4 K	p or f	Perovskite	[167]
$PrOs_4Sb_{12}$	1.85 K	line nodes?	Skutterudite	[168]
$Na_xCoO_{2-y}\cdot H_2O$	5 K	p?	Triangular lattice	[169]
$Ba_{1-x}K_xBiO_3$	30 K	s	Perovskite	[170]
MgB_2	39 K	s	Hexagonal	[171]
$La_{2-x}Sr_xCuO_4$	36 K	d	Perovskite	
$YBa_2Cu_3O_{6+x}$	90 K	d	Perovskite	
$Tl_2Ba_2Ca_{n-1}Cu_nO_{2n+4}$	125 K	d	Perovskite	
$HgBa_2Ca_{n-1}Cu_nO_{2n+2+\delta}$	135 K	d	Perovskite	
$LaO_{1-x}F_xFeAs$	26 K		ZrCuSiAs type	[172]
$NdFeAsO_{1-y}$	54 K		ZrCuSiAs type	[173]
H_3S	203 K	s	(under pressure)	[81]
LaH_{10}	260 K	s	(under pressure)	[82,83,174,175]

2.3. Superconductivity in Strongly Correlated Electron Systems

The possibility of superconductivity in strongly correlated electron systems has been discussed intensively. The perturbative calculations such as the fluctuation-exchange approximation (FLEX) have been performed to investigate the superconducting ground state [176–178]. There were, however, the results by quantum Monte Carlo methods, which did not support the existence of high-temperature superconductivity in the two-dimensional Hubbard model [32,33,45]. In quantum Monte Carlo calculations, the strength of the Coulomb interaction U is not large enough because the range of accessible U is very restricted. It is now certain that there is a superconducting phase in the strongly correlated region [50]. The simplest wave function of superconducting state with strong electron correlation is the Gutzwiller-projected BCS wave function:

$$\psi_{BCS-G} = P_G \prod_{\mathbf{k}} (u_{\mathbf{k}} + v_{\mathbf{k}} c^{\dagger}_{\mathbf{k}\uparrow} c^{\dagger}_{-\mathbf{k}\downarrow}) |0\rangle, \tag{14}$$

where $u_{\mathbf{k}}$ and $v_{\mathbf{k}}$ are BCS parameters and P_G is the Gutzwiller operator to control the on-site electron correlation. P_G is written as

$$P_G = \prod_{j} (1 - (1-g) n_{j\uparrow} n_{j\downarrow}), \tag{15}$$

where g is a variational parameter in the range of $0 \le g \le 1$. The ratio of $u_{\mathbf{k}}$ and $v_{\mathbf{k}}$ is given as

$$\frac{v_{\mathbf{k}}}{u_{\mathbf{k}}} = \frac{\Delta_{\mathbf{k}}}{\zeta_{\mathbf{k}} + (\zeta_{\mathbf{k}}^2 + \Delta_{\mathbf{k}}^2)^{1/2}}, \tag{16}$$

where $\zeta_{\mathbf{k}}$ denotes the electron dispersion relation measured from the Fermi energy and $\Delta_{\mathbf{k}}$ is the gap function. We use the following form for the gap function in the two-dimensional case:

$$\Delta_{\mathbf{k}} = \Delta(\cos k_x - \cos k_y) \quad d - \text{wave}, \tag{17}$$

$$\Delta_{\mathbf{k}} = \Delta(\cos k_x + \cos k_y) \quad \text{anisotropic} - s - \text{wave}, \tag{18}$$

$$\Delta_{\mathbf{k}} = \Delta \quad \text{isotropic } s - \text{wave}. \tag{19}$$

Δ is a constant and is treated as a variational parameter. The wave function ψ_{BCS-G} is just the wave function that Anderson proposed as a wave function of the resonate-valence-bond (RVB) state [72].

It has been shown that the ground-state energy has a minimum at finite Δ for the BCS-Gutzwiller wave function with d-wave symmetry in the two-dimensional Hubbard model by using the variational Monte Carlo method [37]. The superconducting condensation energy E_{cond} per site in the limit of large system size was estimated as [37,38]

$$E_{cond}/N \simeq 0.2 \text{ meV}, \tag{20}$$

where the transfer integral t is set at 0.5 eV. The similar result was obtained for the three-band d-p model [18]. Thus, the condensation energy per atom is of the order of 10^{-4} eV.

The superconducting condensation energy E_{cond} for cuprate high-temperature superconductors was evaluated by using the result of specific heat measurement for YBCO as 0.17–0.26 meV per Cu atom [37,179]. The estimation of E_{cond} from the data of critical magnetic field gives the similar result [180]. The obtained results by theoretical calculations and experimental measurements are very close each other. This agreement is very remarkable. Thus, this value indicates the characteristic energy for cuprate high-temperature superconductors. This result may support that the superconductivity in cuprate high temperature superconductors is caused by the strong electron correlation and the 2D Hubbard model includes essential ingredients.

3. Part II. Mechanism of Superconductivity in Cuprates

We discuss the mechanism of superconductivity in this part. We show numerical results obtained by using the optimized wave functions.

3.1. Model for High-T_c Cuprates

The Hamiltonian of the d-p model for high-T_c cuprates is

$$
\begin{aligned}
H_{dp} &= \epsilon_d \sum_{i\sigma} d_{i\sigma}^\dagger d_{i\sigma} + \epsilon_p \sum_{i\sigma}(p_{i+\hat{x}/2\sigma}^\dagger p_{i+\hat{x}/2\sigma} + p_{i+\hat{y}/2\sigma}^\dagger p_{i+\hat{y}/2\sigma}) \\
&+ t_{dp}\sum_{i\sigma}[d_{i\sigma}^\dagger(p_{i+\hat{x}/2\sigma} + p_{i+\hat{y}/2\sigma} - p_{i-\hat{x}/2\sigma} - p_{i-\hat{y}/2\sigma}) + \text{h.c.}] \\
&+ t_{pp}\sum_{i\sigma}[p_{i+\hat{y}/2\sigma}^\dagger p_{i+\hat{x}/2\sigma} - p_{i+\hat{y}/2\sigma}^\dagger p_{i-\hat{x}/2\sigma} - p_{i-\hat{y}/2\sigma}^\dagger p_{i+\hat{x}/2\sigma} + p_{i-\hat{y}/2\sigma}^\dagger p_{i-\hat{x}/2\sigma} + \text{h.c.}] \\
&+ t_d' \sum_{\langle\langle ij\rangle\rangle\sigma} \epsilon_{ij}(d_{i\sigma}^\dagger d_{j\sigma} + \text{h.c.}) + U_d \sum_i d_{i\uparrow}^\dagger d_{i\uparrow} d_{i\downarrow}^\dagger d_{i\downarrow} \\
&+ U_p \sum_i (n_{i+\hat{x}/2\uparrow}^p n_{i+\hat{x}/2\downarrow}^p + n_{i+\hat{y}/2\uparrow}^p n_{i+\hat{y}/2\downarrow}^p).
\end{aligned}
\tag{21}
$$

Since we use the hole picture in this paper, $d_{i\sigma}$ and $d_{i\sigma}^\dagger$ represent the operators for the d hole. $p_{i\pm\hat{x}/2\sigma}$ and $p_{i\pm\hat{x}/2\sigma}^\dagger$ denote the operators for the p holes at the site $R_{i\pm\hat{x}/2}$, and in a similar way $p_{i\pm\hat{y}/2\sigma}$ and $p_{i\pm\hat{y}/2\sigma}^\dagger$ are defined. $n_{i+\hat{x}/2\sigma}^p$ and $n_{i+\hat{y}/2\sigma}^p$ are the number operators of p holes at $R_{i+\hat{x}/2}$ and $R_{i+\hat{y}/2}$, respectively. t_{dp} is the transfer integral between adjacent Cu and O orbitals and t_{pp} is that between nearest p orbitals. t_d' indicates that between d orbitals where $\langle\langle ij\rangle\rangle$ denotes a next nearest-neighbor pair of copper sites. ϵ_{ij} takes the values ± 1 (See Figure 1). This value is determined from the sign of the transfer integral between next nearest-neighbor d orbitals. U_d indicates the strength of the on-site Coulomb repulsion between d holes and U_p is that between p holes.

The values of band parameters were evaluated by several works [181–185]. We show an example: $U_d = 10.5$, $U_p = 4.0$ and $U_{dp} = 1.2$ eV [182]. Here, U_{dp} is the nearest-neighbor Coulomb interaction between holes on adjacent Cu and O orbitals and is small compared to U_d. U_{dp} is neglected in this paper. We write $\Delta_{dp} = \epsilon_p - \epsilon_d$. The number of sites is denoted as N, and the energy is measured in units of t_{dp}.
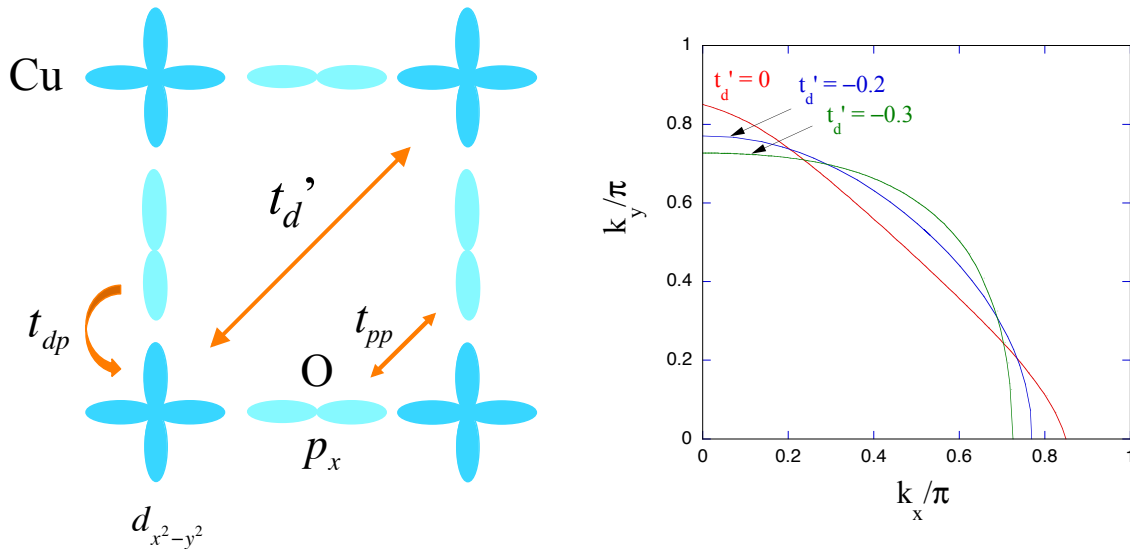

Figure 1. (**Left**) The transfer integral t_d' in the CuO$_2$ plane. t_{dp} and t_{pp} are conventionally defined. (**Right**) Fermi surface of the d-p model with the hole density 0.13 [74]. We put $t_{pp} = 0.4t_{dp}$ and $\epsilon_p - \epsilon_d = 2t_{dp}$ for $t_d' = 0$, $-0.2t_{dp}$ and $-0.3t_{dp}$.

3.2. Optimization Variational Monte Carlo Method

3.2.1. Off-Diagonal Wave Function

The Gutzwiller wave function is

$$\psi_G = P_G \psi_0, \tag{22}$$

where ψ_0 is a one-particle state. Our purpose is to improve the Gutzwiller function. We multiply the Gutzwiller function by an exponential-type operator. The wave function is given as as [50,73,186–190]

$$\psi_\lambda = \exp(-\lambda K)\psi_G, \tag{23}$$

where K denotes the kinetic part of the Hamiltonian. λ is a newly introduced real variational parameter [41,73,187,191]. There are other methods to improve the Gutzwiller function [43,192]. The following Jastrow operator is used [43],

$$P_{Jdh} = \prod_j \left(1 - (1 - \eta) \prod_\tau \left[d_j(1 - e_{j+\tau}) + e_j(1 - d_{j+\tau}) \right] \right), \tag{24}$$

where d_j is the operator for the doubly-occupied site given as $d_j = n_{j\uparrow} n_{j\downarrow}$ and e_j is that for the empty site given by $e_j = (1 - n_{j\uparrow})(1 - n_{j\downarrow})$. η is the variational parameter in the range of $0 \leq \eta \leq 1$. The wave function is

$$\psi_\eta = P_{Jdh} \psi_G. \tag{25}$$

In this paper, we use the wave function of exponential type in Equation (23) because the energy is further lowered when we use this wave function [50]. The wave function for the d-p model is formulated similarly. An initial state ψ_0 contains many variational parameters ($\tilde{t}_{dp}, \tilde{t}_{pp}, \tilde{t}'_d$, and $\tilde{\epsilon}_p - \tilde{\epsilon}_d$):

$$\psi_0 = \psi_0(\tilde{t}_{dp}, \tilde{t}_{pp}, \tilde{t}'_d, \tilde{\epsilon}_p - \tilde{\epsilon}_d). \tag{26}$$

We use $\tilde{t}_{dp} = t_{dp}$ as the energy unit. We consider the following wave function that is improved from the Gutzwiller wave function [50,73,186–190]:

$$\psi_\lambda = \exp(-\lambda K)\psi_G. \tag{27}$$

The expectation values are evaluated by using the auxiliary field method [73,191]. The kinetic part K also contains the band parameters t_{pp}, t'_d and $\epsilon_p - \epsilon_d$ as variational parameters:

$$K = K(\hat{t}_{pp}, \hat{t}'_d, \hat{\epsilon}_p - \hat{\epsilon}_d). \tag{28}$$

We take $\hat{t}_{pp} = \tilde{t}_{pp}$, $\hat{t}'_d = \tilde{t}'_d$ and $\hat{\epsilon}_p - \hat{\epsilon}_d = \tilde{\epsilon}_p - \tilde{\epsilon}_d$, for simplicity. Thus, we have g, $\tilde{t}_{pp}$, $\tilde{t}'_d$, $\hat{\epsilon}_p - \hat{\epsilon}_d = \tilde{\epsilon}_p - \tilde{\epsilon}_d$, and λ as variational parameters. The expectation values for this type of wave function are calculated on the basis of the variational Monte Carlo method. One can evaluate the expectation value correctly within statistical errors.

3.2.2. Antiferromagnetic Wave Function

The AF one-particle state ψ_{AF} is formulated by the eigenfunction of the AF trial Hamiltonian:

$$H_{AF} = \sum_{ij\sigma} t_{ij} c^\dagger_{i\sigma} c_{j\sigma} - \Delta_{AF} \sum_{i\sigma} (-1)^{x_i + y_i} \sigma n_{i\sigma}, \tag{29}$$

where Δ_{AF} is the AF order parameter and (x_i, y_i) represents the coordinates of the site i. With ψ_{AF}, the wave function is given as

$$\psi_{\lambda,AF} = \exp(-\lambda K) P_G \psi_{AF}. \tag{30}$$

3.2.3. Superconducting Wave Function

We start from the BCS wave function

$$\psi_{BCS} = \prod_k (u_k + v_k c_{k\uparrow}^\dagger c_{-k\downarrow}^\dagger)|0\rangle, \tag{31}$$

with coefficients u_k and v_k satisfying $u_k^2 + |v_k|^2 = 1$. We choose $u_k/v_k = \Delta_k/(\xi_k + \sqrt{\xi_k^2 + \Delta_k^2})$ for the gap function Δ_k and $\xi_k = \epsilon_k - \mu$. We assume $\Delta_k = \Delta_{SC}(\cos k_x - \cos k_y)$. The Gutzwiller-projected BCS wave function is

$$\psi_{G-BCS} = P_{N_e} P_G \psi_{BCS}, \tag{32}$$

where P_{N_e} indicates the operator to extract the state with N_e electrons. The exponential-BCS wave function is given by

$$\psi_\lambda = e^{-\lambda K} P_G \psi_{BCS}. \tag{33}$$

In this wave function, we perform the electron–hole transformation for down-spin electrons:

$$d_k = c_{-k\downarrow}^\dagger, \quad d_k^\dagger = c_{-k\downarrow}; \tag{34}$$

and not for up-spin electrons: $c_k = c_{k\uparrow}$. The electron pair operator $c_{k\uparrow}^\dagger c_{-k\downarrow}^\dagger$ denotes the hybridization operator $c_k^\dagger d_k$ in this formulation.

3.3. Correlated Superconductivity

We first discuss the superconducting (SC) state in the two-dimensional Hubbard model. In the optimization Monte Carlo method, the SC state becomes indeed stable when the Coulomb interaction U is large to be of the order of the bandwidth. We show the ground-state energy as a function of the superconducting order parameter Δ in Figure 2 (left). The simple Gutzwiller-projected BCS wave function predicted the possibility of superconductivity in the Hubbard model, and the improved wave function also shows a stability of the SC state.
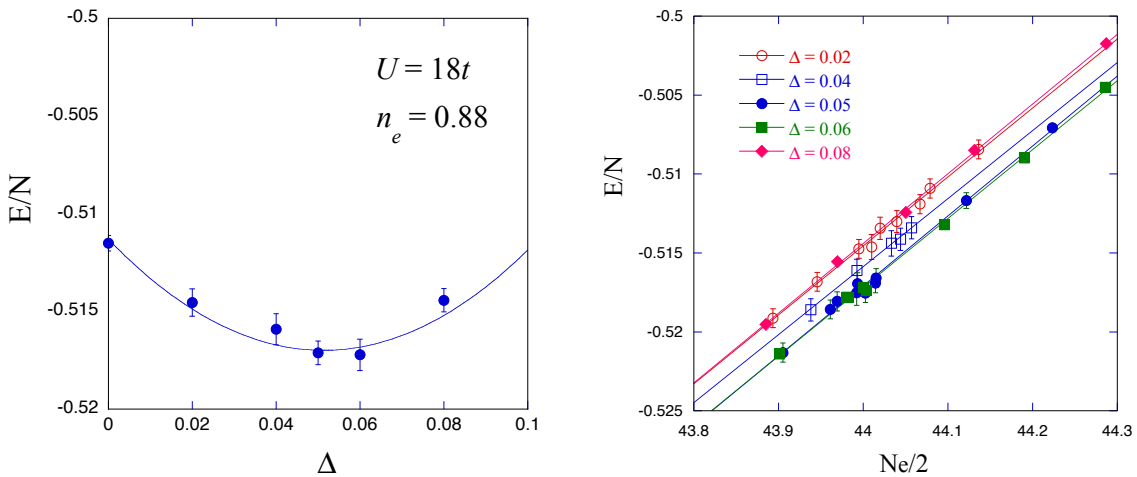

Figure 2. (**Left**) The ground-state energy as a function of the superconducting gap Δ for the optimized wave function ψ_λ for the Hubbard model on a 10×10 lattice with $U/t = 18$ and $t' = 0$. The electron density is $n_e = 0.88$. (**Right**) The ground-state energy as a function of the electron number where Δ is fixed for each line [50].

We show the SC and antiferromagnetic (AF) order parameters as a function of U in Figure 3. The AF order parameter has a peak when $U/t \sim 10$, which is of the order of the bandwidth, and the SC

one also has a peak at U_c that is greater than the bandwidth. This indicates that there is the possibility of high-temperature superconductivity in the strongly correlated region.
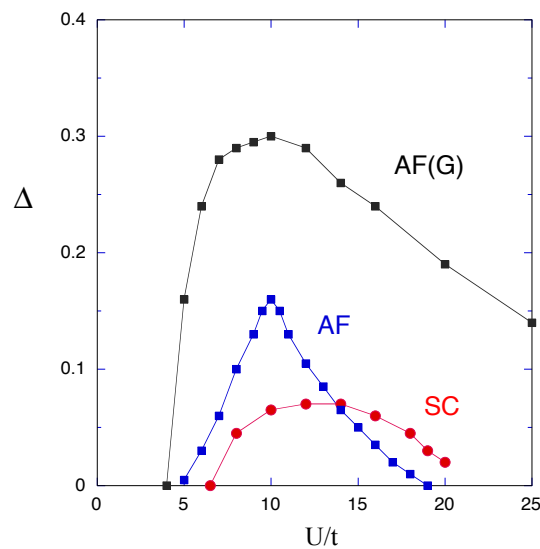

Figure 3. AF and SC order parameters as a function of U/t when $N_e = 88$ for the 2D Hubbard model on a 10×10 lattice. The periodic boundary conditions are periodic in one direction and antiperiodic in the other direction [50]. AF(G) indicates the result obtained for the simple Gutzwiller function.

The AF correlation is maximized at $U \sim U_c$ and decreases when U is larger than U_c. We show schematic pictures in Figure 4, where the SC condensation energy as a function of U is shown in the left panel, and the AF and SC gap functions are shown in the right panel. There is a crossover from weakly correlated region to the strongly correlated region. The superconducting state is most favorable when the AF correlation is gradually suppressed in the strongly correlated region. Thus, high temperature superconductivity is highly promising in the strongly correlated region where U is as large as the bandwidth D or larger than D.
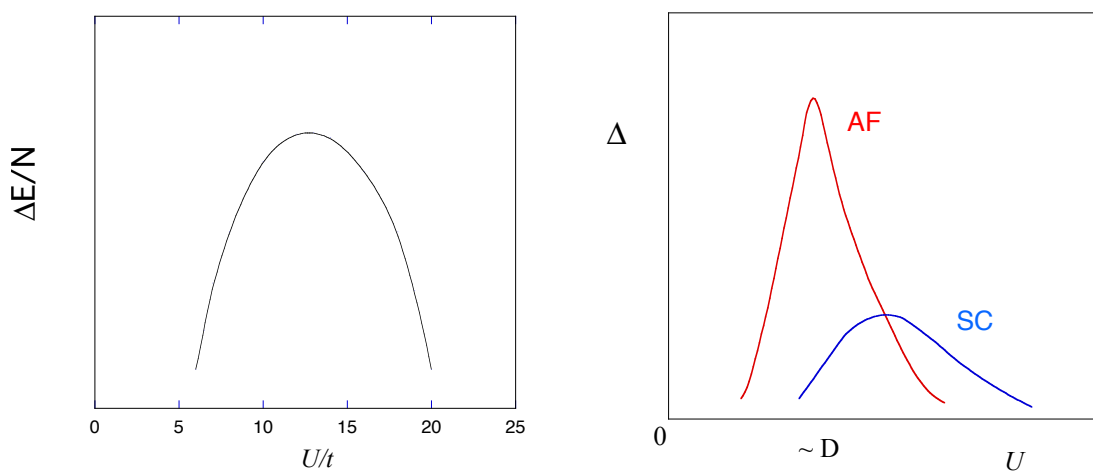

Figure 4. (**Left**) A schematic picture of the superconducting condensation energy as function of U for the 2D Hubbard model. (**Right**) A schematic picture of the gap function of AF and AC states as a function of U for the 2D Hubbard model.

3.4. Stability of Antiferromagnetic State

3.4.1. Hubbard Model

Let us examine the stability of AF state. There are two parameters U and t', and there is the AF region in the parameter space. High temperature superconductivity is expected near the boundary between the AF phase and the paramagnetic phase. We show the AF condensation energy ΔE_{AF} as a function of $1 - n_e$ in Figure 5a for $t' = 0$ and Figure 5b for $t' = -0.2t$. The AF region becomes larger as $|t'|$ increases. When $t' = -0.2t$, the AF region extends up to about 20% doping. From the competition between superconductivity and AF order, $t' = 0$ is most favorable for superconductivity.
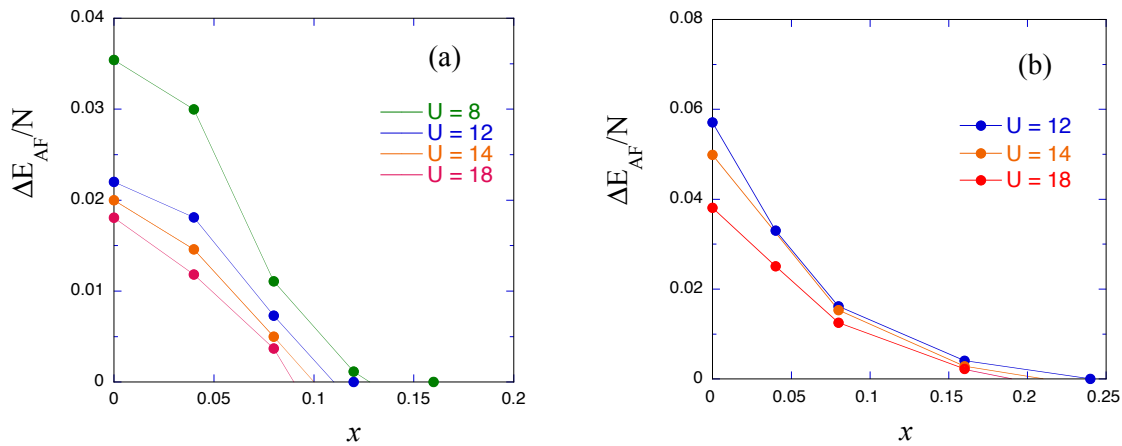
Figure 5. AF condensation energy ΔE_{AF} as a function of the hole doping rate $x = 1 - n_e$ on a 10×10 lattice for: $t' = 0$ (**a**); and $t' = -0.2t$ (**b**) [75]. We put $U/t = 12, 14$ and 18.

3.4.2. Three-Band d-p Model

In general, in the three-band d-p model, the AF correlation is very strong and the AF state is more stable than in the single-band Hubbard model. This is because d electrons are localized and easily form magnetic order [13]. To investigate the possibility of high temperature superconductivity in the d-p model, it is necessary to reveal regions with weak AF order. There are many parameters in the d-p model to control the strength of the AF correlation. Among them, the Coulomb repulsion between d electrons U_d, the level difference $\Delta_{dp} = \epsilon_p - \epsilon_d$, and the hole density x are important. The AF region is shown in Figure 6 where U_d and $\epsilon_p - \epsilon_d$ are varied, and the hole density is fixed at 0.1875. The AF region increases when the hole density decreases. We expect that high temperature superconductivity will occur near the boundary between AFM and PM regions. This boundary exists in the region when Δ_{dp} is small. High temperature superconductivity is likely occur when Δ_{dp} is small. There is a "on-site attractive region" when Δ_{dp} is large where two d electrons prefer to occupy the same site. In this region, a charge-density wave or an s-wave superconducting state will be realized.

We proposed to introduce the transfer integral t'_d to control the strength of AF correlation [74]. We show the AF region at half-filling in the $t_{pp} - t'_d$ plane in Figure 7. As $-t'_d$ increases, there is a phase transition from the AF insulator to the paramagnetic insulator (PMI). We expect that t'_d and t_{pp} will play an important role to suppress AF correlation when holes are doped in the d-p model.
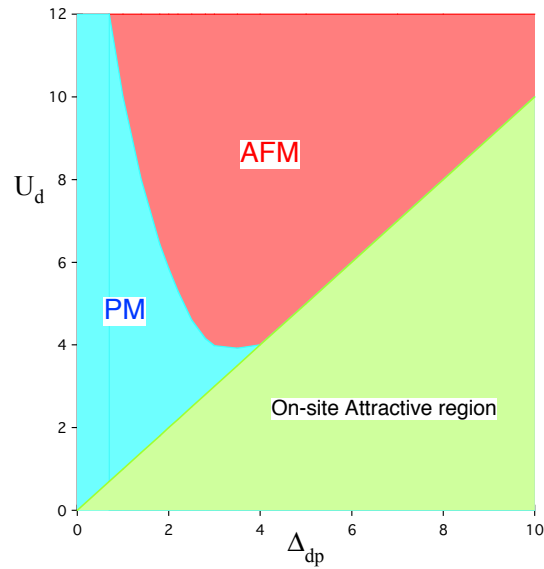
Figure 6. Antiferromagnetic and paramagnetic regions in the plane of U_d and $\Delta_{dp} = \epsilon_p - \epsilon_d$ for the d-p model. We put $t_{pp} = 0.4$ and $t'_d = 0$. There are 76 holes on a 8×8 lattice with 192 atoms in total. The energy unit is given by t_{dp}. AFM and PM denote the antiferromagnetic metal and paramagnetic metal, respectively. There is a "negative-U" region when the level difference is large where two d electrons prefer to occupy the same site. The ground state may be a charge-density wave state or an *s*-wave superconducting state. This is not clear yet.
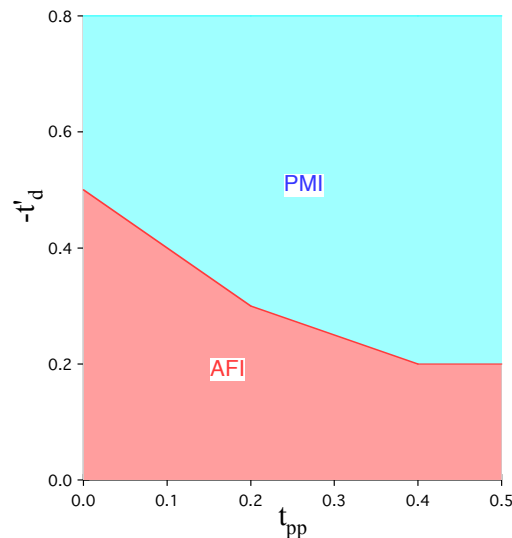
Figure 7. AF and paramagnetic insulator phases for the d-p model on a 6×6 lattice [193]. Parameters are $U_d = 8t_{dp}$, $U_p = 0$, $\epsilon_p - \epsilon_d = t_{dp}$.

3.5. Phase Diagram for the Hubbard Model

We discuss the phase diagram when carrier holes are doped in the CuO$_2$ plane. We evaluate the energy lowering when we include the order parameter Δ. We define

$$\Delta E = E(\Delta = 0) - E(\Delta_{min}), \tag{35}$$

where $E(\Delta)$ takes a minimum at $\Delta = \Delta_{min}$. We show ΔE as a function of the hole doping rate x in Figure 8 where we put $U/t = 18$ and $t' = 0$. This phase diagram contains several interesting features. There are three phases: antiferromagnetic insulator (AFI), coexistent state (AFSC) and superconducting

phase (SC). When the hole doping rate x is large, e.g., $x > 0.09$, the pure d-wave stat is stable. There is the possibility of high (and room) temperature superconductivity in this phase. In the underdoped region, approximately $0.06 < x < x_{dSC}$ with $0.08 < x_{dSC} < 0.09$, there is the coexistent state of antiferromagnetism and superconductivity. This is the mixed phase of AF and SC. x_{dSC} could not be determined precisely. There is the possibility that both the AFSC and SC states are found for $x_{dSC} < x < 0.09$, but the SC solution will have lower energy. There is the AFSC-SC transition at $x = x_{dSC}$. The AFI state exists near half-filling for about $x < 0.06$, where doped holes form clusters and localize.
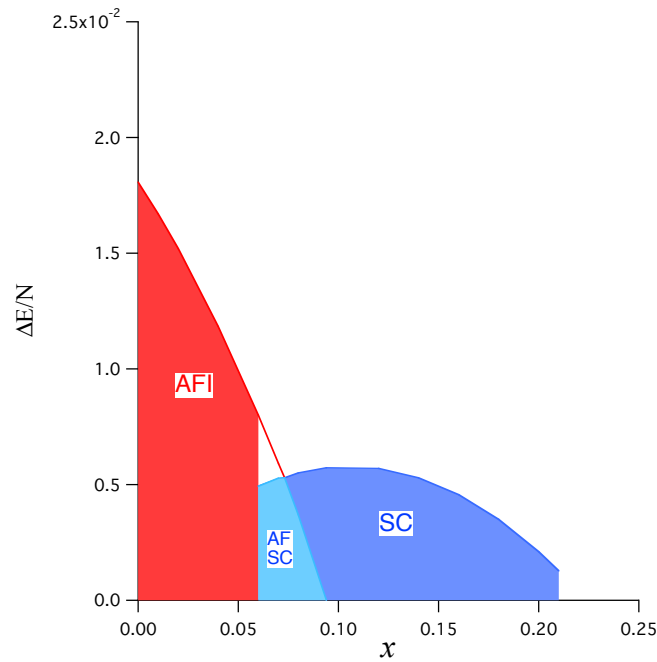

Figure 8. The condensation energy per site for the two-dimensional Hubbard model as a function of the hole doping rate x. The calculation was carried out on a 10×10 lattice. AFI indicates the antiferromagnetic insulating state and SC denotes the d-wave SC phase. There is the coexistent state indicated as AF-SC between these states. Parameters are $t' = 0$ and $U/t = 18$.

The existence of AFI phase is closely related to the phase separation [140,141] when the hole density is very small. In the phase-separated phase, the doped holes are localized and cannot be conductive. The existence of AFI phase is determined by the quantity

$$\delta^2 E(N_e) \equiv [E(N_e + \delta N_e) - 2E(N_e) + E(N_e - \delta N_e)]/(\delta N_e)^2, \tag{36}$$

where $E(N_e)$ is the ground-state energy with N_e electrons. $\delta^2 E(N_e)$ is approximately the second derivative of the energy $E(N_e)$ and is proportional to the charge susceptibility. When $\delta^2 E(N_e)$ is negative, the phase separation occurs. As shown in Figure 8, the phase separation occurs for $x < 0.06$. Concerning the phase separation, the parameter t' is important because the phase separation region decreases as $-t'$ increases. Thus, the AFI phase will decrease as $-t'$ increases. The phase separation disappears for $t' = -0.2t$.

4. Summary

We have discussed the possibility of high temperature superconductivity in many-electron systems. The critical temperature T_c may increase as the characteristic energy of the interaction increases. Empirically, T_c is proportional to the inverse of the effective mass of electrons. T_c is low when the effective mass is very heavy. A candidate of high (room) temperature superconductivity

may be in materials with strong electron correlation and with small effective mass enhancement. From this view point, the repulsive Coulomb interaction can be a candidate of the origin of high temperature superconductivity.

We have shown phase diagrams for the 2D Hubbard model and the three-band d-p model. The diagram in Figure 8 exhibits the characteristic property of cuprate superconductors. This supports that the origin of high temperature superconductivity is the strong correlation between electrons. That is, the mechanism of high-T_c superconductivity is the electron-pair formation due to the strong on-site repulsive Coulomb interaction. The competition between antiferromagnetism and superconductivity is important in realizing high temperature superconductivity. High-T_c superconductivity is expected in the region near the boundary between AF phase and paramagnetic phase. In the phase diagram for the Hubbard model, the SC phase exists near the AF phase, and AF order and superconductivity coexist where the doping rate is approximately $0.05 \sim 0.06 < x < x_{dSC}$ and $0.08 < x_{dSC} < 0.09$. We expect that this coexistence may be related to anomalous metallic behavior in the underdoped region. The AF phase near half-filling is insulating, which is approximately for $x < 0.06$. There is the pure d-wave phase for $x > x_{dSC}$.

In the d-p model, the AF region exists in the multi-dimensional parameter space. The AF-PM boundary is a multi-dimensional region in this space. Since we expect that superconductivity occurs near the boundary, high temperature superconductivity is more likely to occur in the d-p model. There is the AF–PM boundary when the level difference Δ_{dp} is small. Thus, T_c of high temperature cuprates will be high when Δ_{dp} is small. This tendency is consistent with experimental T_c of cuprates.

We give a comment on the crossover between weakly correlated region and strongly correlated region. We expect that this crossover is universal in the sense that similar phenomena occur in nature. There may be a universal class. It will include the Kondo effect [194–196], QCD [197], BCS-BEC crossover [198], sine-Gordon model [199–202], and Gross–Neveu model [203].

Conflicts of Interest: The author declares no conflict of interest.

Abbreviations

The following abbreviations are used in this manuscript:

OVMC	optimization variational Monte Carlo method
AF	antiferromagnetic
SC	superconductivity or superconducting
2D	two-dimensional
AFI	antiferromagnetic insulator
PI	paramagnetic insulator

References

1. Bednorz, J.B.; Müller, K.A. Possible high T$_c$ superconductivity in the Ba-La-Cu-O system. *Z. Phys. B Condens. Matter* **1986**, *B64*, 189–193. [CrossRef]
2. Keimer, B.; Kivelson, S.A.; Norman, M.R.; Uchida, S.; Zaanen, J. From quantum matter to high-temperature superconductivity in copper oxides. *Nature* **2015**, *518*, 179. [CrossRef] [PubMed]
3. Rybicki, D.; Jurkutat, M.; Reichart, S.; Kapusta, C.; Haase, J. Perspective on the phase diagram of cuprate high-temperature superconductors. *Nat. Commun.* **2016**, *7*, 11413. [CrossRef] [PubMed]
4. Cooper, L.N. Bound Electron Paira in a Degenerate Fermi Gas. *Phys. Rev.* **1956**, *104*, 1189. [CrossRef]
5. Bardeen, J.; Cooper, L.N.; Schrieffer, J.R. Microscopic Theory of Superconductivity. *Phys. Rev.* **1957**, *106*, 162. [CrossRef]
6. Bardeen, J.; Cooper, L.N.; Schrieffer, J.R. Theory of Superconductivity. *Phys. Rev.* **1957**, *108*, 1175. [CrossRef]

7.   Emery, V.J. Theory of high-T$_c$ superconductivity in oxides. *Phys. Rev. Lett.* **1987**, *58*, 2794. [CrossRef] [PubMed]

8.   Hirsch, J.E.; Loh, E.Y.; Scalapino, D.J.; Tang, S. Pairing interaction in CuO clusters. *Phys. Rev. B* **1989**, *39*, 243. [CrossRef]

9.   Scalettar, R.T.; Scalapino, D.J.; Sugar, R.L.; White, S.R. Antiferromagnetic, charge-transfer, and pairing correlations in the three-band Hubbard model. *Phys. Rev. B* **1991**, *44*, 770. [CrossRef]

10.   Unger, P.; Fulde, P. Spectral function of holes in the Emergy model. *Phys. Rev. B* **1993**, *48*, 16607. [CrossRef]

11.   Oguri, A.; Asahatam, T.; Maekawa, S. Gutzwiller wave function in the three-band Hubbard model: A variational Monte Carlo study. *Phys. Rev. B* **1994**, *49*, 6880. [CrossRef] [PubMed]

12.   Koikegami, S.; Yamada, K. Antiferromagnetic and superconducting correlations on the d-p model. *J. Phys. Soc. Jpn.* **2000**, *69*, 768. [CrossRef]

13.   Yanagisawa, T.; Koike, S.; Yamaji, K. Ground state of the three-band Hubbard model. *Phys. Rev. B* **2001**, *64*, 184509. [CrossRef]

14.   Koikegami, S.; Yanagisawa, T. Superconducting gap of the two-dimensional d-p model with small U$_d$. *J. Phys. Soc. Jpn.* **2001**, *70*, 3499–3502. [CrossRef]

15.   Yanagisawa, T.; Koike, S.; Yamaji, K. Lattice distortions, incommensurability, and stripes in the electronic model for high-T$_c$ cuprates. *Phys. Rev. B* **2003**, *67*, 132408. [CrossRef]

16.   Koikegami, S.; Yanagisawa, T. Superconductivity in Sr$_2$RuO$_4$ mediated by Coulomb scattering. *Phys. Rev. B* **2003**, *67*, 134517. [CrossRef]

17.   Koikegami, S.; Yanagisawa, T. Superconductivity in multilayer perovskite. *J. Phys. Soc. Jpn.* **2006**, *75*, 034715. [CrossRef]

18.   Yanagisawa, T.; Miyazaki, M.; Yamaji, K. Incommensurate antiferromagnetism coexisting with superconductivity in two-dimensional d-p model. *J. Phys. Soc. Jpn.* **2009**, *78*, 031706. [CrossRef]

19.   Weber, C.; Lauchi, A.; Mila, F.; Giamarchi, T. Orbital currents in extended Hubbard model of High-T$_c$ cuprate superconductors. *Phys. Rev. Lett.* **2009**, *102*, 017005. [CrossRef]

20.   Lau, B.; Berciu, M.; Sawatzky, G.A. High spin polaron in lightly doped CuO$_2$ planes. *Phys. Rev. Lett.* **2011**, *106*, 036401. [CrossRef]

21.   Weber, C.; Giamarchi, T.; Varma, C.M. Phase diagram of a three-orbital model for high-T$_c$ cuprate superconductors. *Phys. Rev. Lett.* **2014**, *112*, 117001. [CrossRef] [PubMed]

22.   Avella, A.; Mancini, F.; Paolo, F.; Plekhanov, E. Emery vs. Hubbard model for cuprate superconductors: A composite operator method study. *Eur. Phys. J.* **2013**, *B86*, 265. [CrossRef]

23.   Ebrahimnejad, H.; Sawatzky, G.A.; Berciu, M. Differences between the insulating limit quasiparticles of one-band and three-band cuprate models. *J. Phys. Condens. Matter* **2016**, *28*, 105603. [CrossRef] [PubMed]

24.   Tamura, S.; Yokoyama, H. Variational study of magnetic ordered state in d-p model. *Phys. Procedia* **2016**, *81*, 5–8. [CrossRef]

25.   Hubbard, J. Electron correlations in narrow energy bands. *Proc. R. Soc. Lond.* **1963**, *276*, 238–257.

26.   Hubbard, J. Electron correlations in narrow energy bands III. *Proc. R. Soc. Lond.* **1964**, *281*, 401–419.

27.   Gutzwiller, M.C. Effect of correlation on the ferromagnetism of transition metals. *Phys. Rev. Lett.* **1963**, *10*, 159. [CrossRef]

28.   Ceperley, D.; Chester, G.V.; Kalos, K.H. Monte Carlo simulation of a many-fermion study. *Phys. Rev. B* **1977**, *16*, 3081. [CrossRef]

29.   Gros, C.; Joynt, R.; Rice, T.M. Antiferromagnetic correlations in almost-localized Fermi liquids. *Phys. Rev. B* **1987**, *36*, 381. [CrossRef]

30.   Yokoyama, H.; Shiba, H. Variational Monte Carlo studies of Hubbard model I. *J. Phys. Soc. Jpn.* **1987**, *56*, 1490–1506. [CrossRef]

31.   Giamarchi, T.; Lhuillier, C. Phase diagrams of the two-dimensional Hubbard and t-J models by a variational Monte Carlo study. *Phys. Rev. B* **1991**, *43*, 12943. [CrossRef] [PubMed]

32.   Zhang, S.; Carlson, J.; Gubernatis, J.E. Constrained path Monte Carlo method for fermion ground states. *Phys. Rev. B* **1997**, *55*, 7464. [CrossRef]

33.   Zhang, S.; Carlson, J.; Gubernatis, J.E. Pairing correlation in the two-dimensional Hubbard model. *Phys. Rev. Lett.* **1997**, *78*, 4486. [CrossRef]

34.   Yanagisawa, T.; Shimoi, Y. Exact results in strongly correlated electrons. *Int. J. Mod. Phys.* **1996**, *B10*, 3383–3450. [CrossRef]

35. Yanagisawa, T.; Shimoi, Y. Ground state of the Kondo-Hubbard model at half-filling. *Phys. Rev. Lett.* **1995**, *74*, 4939. [CrossRef] [PubMed]

36. Nakanishi, T.; Yamaji, K.; Yanagisawa, T. Variational Monte Carlo indications of d-wave superconductivity in the two-dimensional Hubbard model. *J. Phys. Soc. Jpn.* **1997**, *66*, 294–297. [CrossRef]

37. Yamaji, K.; Yanagisawa, T.; Nakanishi, T.; Koike, S. Variational Monte Carlo study on the superconductivity in the two-dimensional Hubbard model. *Physica C* **1998**, *304*, 225–238. [CrossRef]

38. Yamaji, K.; Yanagisawa,T.; Koike, S. Bulk limit of superconducting condensation energy in 2D Hubbard model. *Physica B* **2000**, *284–288*, 415–416. [CrossRef]

39. Yamaji, K.; Yanagisawa, T.; Miyazaki, M.; Kadono, R. Superconducting condensation energy of the two-dimensional Hubbard model in the large-negative-t' region. *J. Phys. Soc. Jpn.* **2011**, *80*, 083702. [CrossRef]

40. Hardy, T.M.; Hague, P.; Samson, J.H.; Alexandrov, A.S. Superconductivity in a Hubbard-Fröhlich model in cuprates. *Phys. Rev. B* **2009**, *79*, 212501. [CrossRef]

41. Yanagisawa, T.; Miyazaki, M.; Yamaji, K. Correlated-electron systems and high-temperature superconductivity. *J. Mod. Phys.* **2013**, *4*, 33. [CrossRef]

42. Bulut, N. $d_{x^2-y^2}$ superconductivity and the Hubbard model. *Adv. Phys.* **2002**, *51*, 1587–1667. [CrossRef]

43. Yokoyama, H.; Tanaka, Y.; Ogata, M.; Tsuchiura, H. Crossover of superconducting properties and kinetic-energy gain in two-dimensional Hubbard model. *J. Phys. Soc. Jpn.* **2004**, *73*, 1119–1122. [CrossRef]

44. Yokoyama, H.; Ogata, M.; Tanaka, Y. Mott transitions and *d*-wave superconductivity in half-filled-band Hubbard model on square lattice with geometric frustration. *J. Phys. Soc. Jpn.* **2006**, *75*, 114706. [CrossRef]

45. Aimi, T.; Imada, M. Does simple two-dimensional Hubbard model account for high-T_c superconductivity in copper oxides? *J. Phys. Soc. Jpn.* **2007**, *76*, 113708. [CrossRef]

46. Miyazaki, M.; Yanagisawa, T.; Yamaji, K. Diagonal stripe states in the light-doping region in the two-dimensional Hubbard model. *J. Phys. Soc. Jpn.* **2004**, *73*, 1643–1646. [CrossRef]

47. Yanagisawa, T. Phase diagram of the t-U^2 Hamiltonian of the weak coupling Hubbard model. *New J. Phys.* **2008**, *10*, 023014. [CrossRef]

48. Yanagisawa, T. Enhanced pair correlation functions in the two-dimensional Hubbard model. *New J. Phys.* **2013**, *15*, 033012. [CrossRef]

49. Yokoyama, H.; Ogata, M.; Tanaka, Y.; Kobayashi, K.; Tsuchiura, H. Crossover between BCS superconductor and doped Mott insulator of *d*-wave pairing state in two-dimensional Hubbard model. *J. Phys. Soc. Jpn.* **2013**, *82*, 014707. [CrossRef]

50. Yanagisawa, T. Crossover from wealy to strongly correlated regions in the two-dimensional Hubbard model—Off-diagonal Monte Carlo studies of Hubbard model II—. *J. Phys. Soc. Jpn.* **2016**, *85*, 114707. [CrossRef]

51. Noack, R.M.; White, S.R.; Scalapino, D.J. The doped two-chain Hubbard model. *EPL* **1995**, *30*, 163. [CrossRef]

52. Noack, R.M.; Bulut, N.; Scalapino, D.J.; Zacher, M.J. Enhanced $d_{x^2-y^2}$ pairing correlations in the two-leg Hubbard ladder. *Phys. Rev. B* **1997**, *56*, 7162. [CrossRef]

53. Yamaji, K.; Shimoi, Y.; Yanagisawa, T. Superconductivity indications of the two-chain Hubbard model due to the two-band effect. *Physica C* **1994**, *235*, 2221. [CrossRef]

54. Yanagisawa, T.; Shimoi, Y.; Yamaji, K. Superconducting phase of a two-chain Hubbard model. *Phys. Rev. B* **1995**, *52*, R3860. [CrossRef] [PubMed]

55. Nakano, T.; Kuroki, K.: Onari, S. Superconductivity due to spin fluctuations originating from multiple Fermi surfaces in the double chain superconductor $Pr_2Ba_4Cu_7O_{15-\delta}$. *Phys. Rev. B* **2007**, *76*, 014515. [CrossRef]

56. Koike, S.; Yamaji, K.; Yanagisawa, T. Effect of the medium-range transfer energies to the superconductivity in the two-chain Hubbard model. *J. Phys. Soc. Jpn.* **1999**, *68*, 1657–1663. [CrossRef]

57. Mott, N.F. *Metal-Insulator Transitions*; Taylor and Francis Ltd.: London, UK, 1974.

58. Moriya, T. *Spin Fluctuations in Itinerant Electron Magnetism*; Springer: Berlin, Germany, 1985.

59. Yosida, K. *Theory of Magnetism*; Springer: Berlin, Germany, 1996.

60. Tranquada, J.M.; Axe, J.D.; Ichikawa, N.; Nakamura, Y.; Uchida, S.; Nachumi, B. Neutron-scattering study of stripe-phase order of holes and spins in $La_{1.48}Nd_{0.4}Sr_{0.12}CuO_4$. *Phys. Rev. B* **1996**, *54*, 7489. [CrossRef] [PubMed]

61. Suzuki, T.; Goto, T.; Shinoda, T.; Fukase, T.; Kimura, H.; Yamada, K.: Ohashi, M.; Yamaguchi, Y. Observation of modulated magnetic long-range order in $La_{1.88}Sr_{0.12}CuO_4$. *Phys. Rev. B* **1998**, *57*, R3229. [CrossRef]

62. Yamada, K.; Lee, C.H.; Kurahashi, K.; Wada, J.; Wakimoto, S.; Ueki, S.; Kimura, H.; Endoh, Y.; Hosoya, S.; Shirane, G.; et al. Doping dependence of the spatially modulated dynamical spin correlations and the superconducting-transition temperature in $La_{2-x}Sr_xCuO_4$. *Phys. Rev. B* **1998**, *57*, 6165. [CrossRef]

63. Arai, M.; Nishijima, T.; Endoh, Y.; Egami, T.; Tajima, S.; Tomimoto, K.; Shiohara, Y.; Takahashi, M.; Garrett, A.; Bennington, S.M. Incommensurate spin dynamics of underdoped superconductor $YBa_2Cu_3Y_{6.7}$. *Phys. Rev. Lett.* **1999**, *83*, 608. [CrossRef]

64. Mook, H.A.; Pengcheng, D.; Dogan, F.; Hunt, R.D. One-dimensional nature of the magnetic fluctuations in $YBa_2Cu_3O_{6.6}$. *Nature* **2000**, *404*, 729. [CrossRef] [PubMed]

65. Wakimoto, S.; Birgeneau, R.J.; Kastner, M.A.; Lee, Y.S.; Erwin, R.; Gehring, P.M.; Lee, S.H.; Fujita, M.; Yamada, K.; Endoh, Y.; et al. Direct observation of a one-dimensional static spin modulation in insulating $La_{1.95}Sr_{0.05}CuO_4$. *Phys. Rev. B* **2000**, *61*, 3699. [CrossRef]

66. Bianconi, A.; Saini, N.L.; Lanzara, A.; Missori, M.; Rossetti, T.; Oyanagi, H.; Yamaguchi, H.; Oka, K.; Ito, T. Determination of the local lattice distortions in the CuO_2 plane of $La_{1.85}Sr_{0.15}CuO_4$. *Phys. Rev. Lett.* **1996**, *76*, 3412. [CrossRef] [PubMed]

67. Bianconi, A. Quantum materials: Shape resonances in superstripes. *Nat. Phys.* **2013**, *9*, 536. [CrossRef]

68. Hoffman, J.E.; McElroy, K.; Lee, D.-H.; Lang, K.M.; Eisaki, H.; Uchida, S.; Davis, J.C. Imaging quasiparticle interference in $Bi_2Sr_2CaCu_2O_{8+\delta}$. *Science* **2002**, *295*, 466. [CrossRef] [PubMed]

69. Wise, W.D.; Boyer, M.C.; Chatterjee, K.; Kondo, T.; Takeuchi, T.; Ikuta, J.; Wang, Y.; Hudson, E.W. Charge-density-wave origin of cuprate checkerboard visualized by scanning tunnelling microscopy. *Nat. Phys.* **2008**, *4*, 696. [CrossRef]

70. Hanaguri, T.; Lupien, C.; Kohsaka, Y.; Lee, D.-H.; Azuma, M.; Takano, M.; Takagi, H.; Davis, J. A checkerboard electronic crystal state in lightly hole-doped $Ca_{2-x}Na_xCuO_2Cl_2$. *Nature* **2004**, *430*, 1001. [CrossRef]

71. Miyazaki, M.; Yanagisawa, T.; Yamaji, K. Checkerboard states in the two-dimensional Hubbard model with the Bi2212-type band. *J. Phys. Soc. Jpn.* **2009**, *78*, 043706. [CrossRef]

72. Anderson, P.W. The resonating valence bond states in La_2CuO_4. *Science* **1987**, *253*, 1196. [CrossRef]

73. Yanagisawa, T.; Koike, S.; Yamaji, K. Off-diagonal wave function Monte Carlo Studies of Hubbard model I. *J. Phys. Soc. Jpn.* **1998**, *67*, 3867–3874. [CrossRef]

74. Yanagisawa, T.; Miyazaki, M. Mott transition in cuprate high-temperature superconductors. *EPL* **2014**, *107*, 27004. [CrossRef]

75. Yanagisawa, T. Antiferromagnetism, superconductivity and phase diagram in the two-dimensional Hubbard model—Off-diagonal wave function Monte Carlo studies of Hubbard model III—. *J. Phys. Soc. Jpn.* **2019**, *88*, 054702. [CrossRef]

76. Eliashberg, G.M. Interactions between electrons and lattice vibrations in a superconductor. *Sov. Phys. JETP* **1960**, *11*, 696–702.

77. Carbotte, J.P. Properties of boson-exchange superconductors. *Rev. Mod. Phys.* **1990**, *62*, 1027. [CrossRef]

78. McMillan, W.L. Transition temperature of strong-coupled superconductors. *Phys. Rev.* **1968**, *167*, 331. [CrossRef]

79. Allen, P.B.; Dynea, R.C. Transition temperature of strong-coupled superconductors reanalyzed. *Phys. Rev. B* **1968**, *12*, 905. [CrossRef]

80. Ashcroft, N.W. Metallic hydrogen: A high-temperature superconductor? *Phys. Rev. Lett.* **1968**, *21*, 1748. [CrossRef]

81. Drozdov, A.P.; Eremets, M.I.; Troyan, I.A.; Ksenofontov, V.; Shylin, S.I. Conventional superconductivity at 203 kelvin at high pressures in the sulfur hydride system. *Nature* **2015**, *525*, 73. [CrossRef] [PubMed]

82. Peng, F.; Sun, Y.; Pickard, C.J.; Needs, R.J.; Wu, Q.; Ma, Y. Hydrogen clathrate structures in rare earth hydrides at high pressures: Possible route to room-temperature superconductivity. *Phys. Rev. Lett.* **2017**, *119*, 107001. [CrossRef] [PubMed]

83. Liu, H.; Naumov, I.I.; Hoffmann, R.; Schcroft, N.W.; Hemley, R.J. Potential high-T_c superconducting lanthanum and yttrium hydrides at high pressure. *Proc. Natl. Acad. Sci. USA* **2017**, *114*, 6990–6995. [CrossRef] [PubMed]

84. Innocenti, D.; Poccia, N.; Ricci, A.; Valletta, A.; Caprara, S.; Perali, A.; Bianconi, A. Resonant and crossover phenomena in a multiband superconductor: Tuning the chemical potential near a band edge. *Phys. Rev. B* **2010**, *82*, 184528. [CrossRef]

85. Mazziotti, M.V.; Valletta, A.; Campi, G.; Innocenti, D.; Perali, A.; Bianconi, A. Possible Fano resonance for high-T_c multi-gap superconductivity in p-Terphenyl doped at the Lifshitz transition. *EPL* **2017**, *118*, 37003. [CrossRef]

86. Moskalenko, V.A. *Fiz. Metal Mallored.* **1959**, *8*, 2518.

87. Suhl, H.; Mattias, B.T.; Walker, L.R. Bardeen-Cooper-Schrieffer theory of superconductivity in the case of overlapping bands. *Phys. Rev. Lett.* **1959**, *3*, 552. [CrossRef]

88. Peretti, J. Superconductivity of transition elements. *Phys. Lett.* **1962**, *2*, 275. [CrossRef]

89. Kondo, J. Superconductivity in transition metals. *Prog. Theor. Phys.* **1963**, *29*, 1–9. [CrossRef]

90. Stanev, V.; Tesanovic, Z. Three-band superconductivity and the order parameter that breaks time-reversal symmetry. *Phys. Rev. B* **2010**, *81*, 134522. [CrossRef]

91. Tanaka, Y.; Yanagisawa, T. Chiral ground state in three-band superconductors. *J. Phys. Soc. Jpn.* **2010**, *79*, 114706. [CrossRef]

92. Tanaka, Y.; Yanagisawa, T. Chiral state in three-gap superconductors. *Solid State Commun.* **2010**, *150*, 1980–1982. [CrossRef]

93. Dias, R.G.; Marques, A.M. Frustrated multiband superconductivity. *Superconduct. Sci. Technol.* **2011**, *24*, 085009. [CrossRef]

94. Yanagisawa, T.; Tanaka, Y.; Hase, I.; Yamaji, K. Vortices and chirality in multi-band superconductors. *J. Phys. Soc. Jpn.* **2012**, *81*, 024712. [CrossRef]

95. Hu, X.; Wang, Z. Stability and Josephson effect of time-reversal-symmetry-broken multicomponent superconductivity induced by frustrated intercomponent coupling. *Phys. Rev. B* **2012**, *85*, 064516. [CrossRef]

96. Stanev, V. Model of collective modes in three-band superconductors with repulsive interband interactions. *Phys. Rev. B* **2012**, *85*, 174520. [CrossRef]

97. Platt, C.; Thomale, R.; Homerkamp, C.; Zhang, S.C.; Hanke, W. Mechanism for a pairing with time-reversal symmetry breaking in iron-based superconductors. *Phys. Rev. B* **2012**, *85*, 180502. [CrossRef]

98. Maiti, S.; Chubukov, A.V. $s + is$ state with broken time-reversal symmetry in Fe-based superconductors. *Phys. Rev. B* **2013**, *87*, 144511. [CrossRef]

99. Wilson, B.J.; Das, M.P. Time-reversal-symmetry-broken state in the BCS formalism for a multi-band superconductor. *J. Phys. Condens. Matter* **2013**, *25*, 425702. [CrossRef] [PubMed]

100. Ganesh, R.; Baskaran, G.; van den Brink, J.; Efremov, D.V. Theoretical prediction of a time-reversal broken chiral superconducting phase driven by electronic correlations in a single TiSe$_2$ layer. *Phys. Rev. Lett.* **2014**, *113*, 177001. [CrossRef]

101. Yerin, Y.S.; Omelyanchouk, A.N.; Il'ichev, E. Dc SQUID based on a three-band superocnductor with broken time-reversal symmetry. *Superconduct. Sci. Technol.* **2015**, *28*, 095006. [CrossRef]

102. Hillier, A.D.; Quintanilla, J.; Cywinskii, R. Evidence for time-reversal symmetry breaking in the noncentrosymmetric superconductor LaNiC$_2$. *Phys. Rev. Lett.* **2009**, *102*, 117007. [CrossRef]

103. Hase, I.; Yanagisawa, T. Electronic structure of RNiC$_2$ (R = La, Y, and Th). *J. Phys. Soc. Jpn.* **2009**, *78*, 084724. [CrossRef]

104. Yanagisawa, T.; Hase, I. Massless modes and abelian gauge fields in multi-band superconductors. *J. Phys. Soc. Jpn.* **2013**, *82*, 124704. [CrossRef]

105. Lin, S.Z.; Hu, X. Phase solitons in multi-band superconductors with and without time-reversal symmetry. *New J. Phys.* **2012**, *14*, 063021. [CrossRef]

106. Kobayashi, K.; Machida, M.; Ota, Y.; Nori, F. Massless collective excitations in frustrated multiband superconductors. *Phys. Rev. B* **2013**, *88*, 224516. [CrossRef]

107. Koyama, T. Collective modes in multiband superconductors: Rigorous study based on the Ward-Takahashi relations. *J. Phys. Soc. Jpn.* **2014**, *83*, 074715. [CrossRef]

108. Yanagisawa, T.; Tanaka, Y. Fluctuation-induced Nambu-Goldstone bosons in a Higs-Josephson model. *New J. Phys.* **2014**, *16*, 123014. [CrossRef]

109. Tanakai, Y.; Hase, I.; Yanagisawa, T.; Kato, G.; Nishio, T.; Arisawa, S. Current-induced massless mode of the interband phase difference in two-band superconductors. *Physica C* **2015**, *516*, 10. [CrossRef]

110. Valletta, A.; Bianconi, A.; Perali, A.; Saini, N.L. Electronic and superconducting properties of a superlattice of quantum stripes at the atomic limit. *Z. Physik B Condens. Matter* **1997**, *104*, 707. [CrossRef]

111. Choi, H.Y.; Yun, J.H.; Bang, Y.; Lee, H.C. Model for the inverse isotope effect of FeAs-based superconductors in the π-phase-shifted pairing state. *Phys. Rev. B* **2009**, *80*, 052505. [CrossRef]

112. Shirage, P.M.; Kihou, K.; Miyazawa, K.; Lee, C.-H.; Kito, H.; Eisaki, H.; Yanagisawa, T.; Tanaka, Y.; Iyo, A. Inverse iron isotope effect on the transition temperature of the (Ba,K)Fe$_2$As$_2$ superconductor. *Phys. Rev. Lett.* **2009**, *103*, 257003. [CrossRef]

113. Yanagisawa, T.; Odagiri, K.; Hase, I.; Yamaji, K.; Shirage, P.M.; Tanaka, Y.; Iyo, A.; Eisaki, H. Isotope effect in multi-band and multi-channel attractive systems and inverse isotope effect in iron-based superconductors. *J. Phys. Soc. Jpn.* **2009**, *78*, 094718. [CrossRef]

114. Perali, A.; Innocenti, D.; Valletta, A.; Bianconi, A. Anomalous isotope effect near a 2.5 Lifshitz transition in a multi-band multi-condensates superconductor made of a superlattice of stripes. *Superconduct. Sci. Technol.* **2012**, *25*, 124002. [CrossRef]

115. Izyumov, Y.A.; Laptev, V.M. Vortex structure in superconductors with a many-component order parameter. *Phase Transit.* **1990**, *20*, 95. [CrossRef]

116. Volovik, G.E. *The Universe in a Helium Droplet*; Oxford University Press: Oxford, UK, 2009.

117. Kuplevakhsky, S.V.; Omelyanchouk, A.N.; Yerin, Y.S. Soliton states in mesoscopic two-band superconducting cylinders. *J. Low Temp. Phys.* **2011**, *37*, 667. [CrossRef]

118. Tanaka, Y.; Yamamori, H.; Yanagisawa, T.; Nishio, T.; Arisawa, S. Experimental formation of a fractional vortex in a superconducting bi-layer. *Physica C* **2018**, *548*, 44. [CrossRef]

119. Yanagisawa, T.; Hase, I.; Tanaka, Y. Massless and quantized modes of kinks in the phase space of superconducting gaps. *Phys. Lett. A* **2018**, *382*, 3483. [CrossRef]

120. Littlewood, P.B.; Varma, C.M. Amplitude collective modes in superconductors and their coupling to charge-density wave. *Phys. Rev. B* **1982**, *26*, 4883. [CrossRef]

121. Cea, T.; Benfatto, L. Nature and Raman signature of the Higgs amplitude modes in the coexisting superconducting and charge-density-wave mode. *Phys. Rev. B* **2014**, *90*, 224515. [CrossRef]

122. Pekker, D.; Varma, C.M. Amplitude/Higgs modes in condensed matter physics. *Annu. Rev. Condens. Matter Phys.* **2015**, *6*, 269–297. [CrossRef]

123. Cea, T.; Castellani, C.; Seibold, G.; Benfatto, L. Nonrelativistic dynamics of the amplitude (Higgs) mode in superconductors. *Phys. Rev. Lett.* **2015**, *115*, 157002. [CrossRef]

124. Koyama, T. Perturbative approach to the collective modes in the TRSB phase of multiband superconductors. *J. Phys. Soc. Jpn.* **2016**, *85*, 064715. [CrossRef]

125. Yanagisawa, T. Fluctuation modes in multi-gap superconductors. In *Vortices and Nanostructured Superconductors*; Crisan, A., Ed.; Springer: Berlin, Germany, 2017.

126. Yanagisawa, T. Nambu-Goldstone bosons characterized by the order parameters in spontaneous symmetry breaking. *J. Phys. Soc. Jpn.* **2017**, *86*, 104711. [CrossRef]

127. Aitchison, I.J.R.; Ao, P.; Thouless, D.; Zhu, X.M. Effective Lagrangian for BCS superconductors at $T = 0$. *Phys. Rev. B* **1995**, *51*, 6531. [CrossRef] [PubMed]

128. Murotani, Y.; Tsuji, N.; Aoki, H. Theory of light-induced resonances with collective Higgs and Leggett modes in multiband superconductors. *Phys. Rev. B* **2017**, *95*, 104503. [CrossRef]

129. Yanagisawa, T. Theory of Green's functions of Nambu-Goldstone and Higgs modes in superconductors. *J. Superconduct. Novel Magn.* **2019**. [CrossRef]

130. Perali, A.; Bianconi, A.; Lanzara, A.; Saini, N.L. The gap amplification at a shape resonance in a superlattice of quantum stripes: A mechanism for high T_c. *Solid State Commun.* **1996**, *100*, 181–186. [CrossRef]

131. Bianconi, A.; Valletta, A.; Perali, A.; Saini, N.L. Superconductivity of s striped phase at the atomic limit. *Physica C* **1998**, *296*, 269–280. [CrossRef]

132. Kusmartsev, F.V.; Di Castro, D.; Bianconi, G.; Bianconi, A. Transformation of strings into an inhomogeneous phase of stripes and itinerant carriers. *Phys. Lett. A* **2000**, *275*, 118. [CrossRef]

133. Müller, K.A.; Zhao, G.M.; Conder, K.; Keller, H. The ratio of small polarons to free carriers in derived from susceptibility measurements. *J. Phys. Condens. Matter* **1998**, *10*, L291. [CrossRef]

134. Bianconi, A. On the Fermi liquid coupled with a generalized Wigner polaronic CDW giving high T_c superconductivity. *Solid State Commun.* **1994**, *91*, 1–5. [CrossRef]

135. Harris, A.B.; Lange, R.V. Single-particle excitations in narrow energy bands. *Phys. Rev.* **1967**, *157*, 295. [CrossRef]

136. Chao, K.A.; Spalek, J.; Oleś, A.M. Kinetic exchange interaction in a narrow s-band. *J. Phys. C* **1977**, *10*, L271. [CrossRef]

137. Chao, K.A.; Spalek, J.; Oleś, A.M. Canonical perturbation expansion of the Hubbard model. *Phys. Rev. B* **1978**, *18*, 3453. [CrossRef]

138. Micnas, R.; Ranninger, J.; Robaszkiewicz, S. Superconductivity in narrow-band systems with local nonretarded attractive interactions. *Rev. Mod. Phys.* **1990**, *62*, 113. [CrossRef]

139. Robaszkiewicz, S.; Pawlowski, G. Effects of finite pair binding energy in a model for a superconductor with local electron pairing. *Physica C* **1993**, *210*, 61–79. [CrossRef]

140. Arrigoni, E.; Strinati, G.C. Doping-induced incommensurate antiferromagnetism in a Mott-Hubbard insulator. *Phys. Rev. B* **1991**, *44*, 7455. [CrossRef] [PubMed]

141. Kapcia, K.; Robaszkiewicz, S.; Micnas, R. Phase separation in a lattice model of a superconductor with pair hopping. *J. Phys. Condens. Matter* **2012**, *24*, 215601. [CrossRef] [PubMed]

142. Feiner, L.F.; Jefferson, J.H.; Raimondi, R. Effective single-band models for high-T_c cuprates I Coulomb interactions. *Phys. Rev. B* **1996**, *53*, 8751. [CrossRef]

143. Kuroki, K.; Onari, S.; Arita, R.; Usui, H.; Tanaka, Y.; Kontani, H.; Aoki, H. Unconventional Pairing Originating from the Disconnected Fermi Surfaces of Superconducting LaFeAsO$_{1-x}$F$_x$. *Phys. Rev. Lett.* **2008**, *101*, 087004. [CrossRef]

144. Grewe, N.; Steglich, F. Heavy fermions. *Handb. Phys. Chem. Of Rare Earths* **1991**, *14*, 343.

145. Hewson, A.C. *The Kondo Problem to Heavy Fermions*; Cambridge University Press: Cambridge, UK, 1993.

146. Onuki, Y. *Physics of Heavy Fermions: Heavy Fermions and Strongly Correlated Electron Systems*; World Scientific Pub Co Inc.: Singapore, 2018.

147. Ishiguro, T.; Yamaji, K.; Saito, G. *Organic Superconductors*; Springer: Berlin, Germany, 2012.

148. Akashi, R.; Kawamura, M.; Tsuneyuki, S.; Nomura, Y.; Arita, R. First-principles study of the pressure and crystal-structure dependences of the superconducting transition temperature in compressed sulfur hydrides. *Phys. Rev. B* **2015**, *91*, 224513. [CrossRef]

149. Steglich, R.; Asrts, J.; Bredl, C.D.; Lieke, W.; Meschede, D.; Franz, W.; Schäfer, H. Superconductivity in the presence of strong Pauli paramagnetism: CeCu$_2$Si$_2$. *Phys. Rev. Lett.* **1979**, *43*, 1892. [CrossRef]

150. Kittaka, S.; Aoki, Y.; Shimura, Y.; Sakakibara, T.; Seiro, S.; Geibel, C.; Steglich, F.; Ikeda, H.; Machida, K. Multiband superconductivity with unexpected deficiency of nodal quasiparticles in CeCu$_2$Si$_2$. *Phys. Rev. Lett.* **2014**, *112*, 0607002. [CrossRef] [PubMed]

151. Stewart, G.R.; Fisk, Z.; Smith, J.L.; Willis, J.O.; Wire, M.S. New heavy-fermion system NpBe$_{13}$ with a comparison to UBe$_{13}$ and PuBe$_{13}$. *Phys. Rev. Lett.* **1984**, *52*, 679. [CrossRef]

152. Ott, H.R.; Rudingier, H.; Delsing, P.; Fisk, Z. Magnetic ground state of a heavy-electron system: U$_2$Zn$_{17}$. *Phys. Rev. Lett.* **1984**, *52*, 1551. [CrossRef]

153. Palstra, T.T.; Menovsky, A.A.; van den Berg, J. Superconducting and magnetic transitions in the heavy-fermion system URu$_{12}$. *Phys. Rev. Lett.* **1985**, *55*, 2727. [CrossRef] [PubMed]

154. Amitsuka, H.; Sato, M.; Metoki, N.; Yokoyama, M.; Kuwahara, K.; Sakakibara, T.; Morimoto, H.; Kawarazaki, S.; Miyako, Y.; Mydosh, J.A. Effect of pressure on tiny antiferromagnetic moment in the heavy-electron compound URu$_2$Si$_2$. *Phys. Rev. Lett.* **1999**, *83*, 5114. [CrossRef]

155. Ohkuni, H.; nada, Y.; Tokiwa, Y.; Sakurai, K.; Settai, R.; Honma, T.; Haga, Y.; Yamamoto, E.; Onuki, Y.; Yamagami, H.; et al. Fermi surface properties and de Haas-van Alphen oscillation in both the normal and superconducting mixed states of URu$_2$Si$_2$. *Philos. Mag.* **1999**, *B79*, 1045.

156. Hedo, M.; Inada, Y.; Yamamoto, E.; Haga, Y.; Onuki, Y.; Aoki, Y.; Matsuda, D.; Sato, H.; Takahashi, S. Superconducting properties of CeRu$_2$. *J. Phys. Soc. Jpn.* **1998**, *67*, 272–279. [CrossRef]

157. Geibel, G.; Schank, C.; Thies, S.; Kitazawa, H.; Bredl, C.D.; Bohm, A.; Rau, M.; Grauel, A.; Caspary, R.; Helfrich, R.; et al. Heavy-fermion superconductivity at $T_=$2K in the antiferromagnet UPd$_2$Al$_3$. *Z. Phys. B* **1991**, *84*, 1–2. [CrossRef]

158. Kyogaku, M.; Kitaoka, Y.; Asayama, K.; Geibel, C.; Schank, C.; Steglich, F. NMR and NQR studies of magnetism and superconductivity in the antiferromagnetic heavy fermion superconductors UM$_2$Al$_3$ (M = Ni and Pd). *J. Phys. Soc. Jpn.* **1993**, *62*, 4016–4030. [CrossRef]

159. Inada, Y.; Yamagami, H.; Haga, Y.; Sakurai, K.; Tokiwa, Y.; Honma, T.; Yamamoto, E.; Onuki, Y.; Yanagisawa, T. Fermi surface and de Haas-van Alphen oscillation in both the normal and superconducting mixed states of UPd$_2$Al$_3$. *J. Phys. Soc. Jpn.* **1999**, *68*, 3643–3654. [CrossRef]

160. Ishida, K.; Mukuda, H.; Kitaoka, Y.; Asayama, K.; Mao, Z.Q.; Mori, Y.; Maeno, Y. Spin-triplet superconductivity in UNi_2Al_3 revealed by the ^{27}Al knight shift measurement. *Phys. Rev. Lett.* **2002**, *89*, 037002. [CrossRef] [PubMed]

161. Petrovic, C.; Pagliuso, P.G.; Hundley, M.F.; Movshovich, R.; Sarrao, J.L.; Thompson, J.D.; Fisk, Z.; Monthoux, P. heavy-fermion superconductivity in $CeCoIn_5$ at 2.3 K. *J. Phys. Condens. Matter* **2001**, *13*, L337. [CrossRef]

162. Izawa, K.; Yamaguchi, H.; Matsuda, Y.; Shishido, H.; Settai, R.; Onuki, Y. Angular position of nodes in the superconducting gap of quasi-2D heavy-fermion superconductor $CeCoIn_5$. *Phys. Rev. Lett.* **2001**, *87*, 057002. [CrossRef] [PubMed]

163. Hegger, H.; etrovic, C.; Moshopoulou, E.G.; Hundley, M.F.; Sarrao, J.L.; Fisk, Z.; Thompson, J.D. Pressure-induced superconductivity in quasi-2D $CeRhIn_5$. *Phys. Rev. Lett.* **2000**, *84*, 4986. [CrossRef] [PubMed]

164. Movshovich, R.; Graf, T.; Mandrus, D.; Thompson, J.D.; Smith, J.L.; Fisk, Z. Superconductivity in heavy-fermion $CeRh_2Si_2$. *Phys. Rev. B* **1996**, *53*, 8241. [CrossRef] [PubMed]

165. Saxena, S.S.; Agarwal, P.; Ahilan, K.; Grosche, F.M.; Haselwimmer, R.K.W.; Steiner, M.J.; Pugh, E.; Walker, I.R.; Julian, S.R.; Monthoux, P.; et al. Superconductivity on the border of itinerant-electron ferromagnetism in UGe_2. *Nature* **2000**, *406*, 587. [CrossRef] [PubMed]

166. Aoki, D.; Huxley, A.; Ressouche, E.; Braithwaite, D.; Flouquet, J.; Brison, J.-P.; Lhotel, E.; Paulsen, C. Coexistence of superconductivity and ferromagnetism in URhGe. *Nature* **2001**, *413*, 613. [CrossRef] [PubMed]

167. Maeno, Y.; Hashimoto, H.; Yoshida, K.; Nishizaki, S.; Fujita, T.; Bednorz, J.G.; Lichtenberg, F. Superconductivity in a layered perovskite without copper. *Nature* **1994**, *372*, 532. [CrossRef]

168. Bauer, E.D.; Frederick, N.A.; Ho, P.-C.; Zapf, V.S.; Maple, M.B. Superconductivity and heavy fermion behavior in $PrOs_4Sb_{12}$. *Phys. Rev. B* **2002**, *65*, R100506. [CrossRef]

169. Takada, K.; Sakurai, H.; Takayama-Muromachi, E.; Izumi, F.; Dilanian, F.A.; Sakai, T. Superconductivity in two-dimensional CoO_2 layers. *Nature* **2003**, *422*, 53. [CrossRef] [PubMed]

170. Chaillout, C.; Remeika, J.P.; Santoro, A.; Mareizo, M. The determination of the Bi valence state in $BaBiO_3$ by neutron powder diffraction data. *Solid State Commun.* **1985**, *56*, 829–831. [CrossRef]

171. Nagamatsu, J.; Nakagawa, N.; Muranaka, T.; Zenitani, Y.; Akimitsu, J. Superconductivity at 39 K in magnesium diboride. *Nature* **2001**, *410*, 63. [CrossRef] [PubMed]

172. Kamihara, Y.; Watanabe, T.; Hirano, M.; Hosono, H. Iron-based layered superconductor $La(O_{1-x}F_x)FeAs$ ($x = 0.05 - 0.12$) with $T_c = 26$ K. *J. Am. Chem. Soc.* **2000**, *130*, 3296. [CrossRef] [PubMed]

173. Kito, H.; Eisaki, H.; Iyo, A. Superconductivity at 54 K in F-free $NdFeAsO_{1-y}$. *J. Phys. Soc. Jpn.* **2008**, *77*, 063707. [CrossRef]

174. Drozdov, A.P.; Minkov, V.S.; Besedin, S.P.; Kong, P.P.; Kuzovnikov, M.A.; Knyazev, D.A.; Eremets, M.I. Superconductivity at 250 K in lanthanum hydride at high pressures. *Nature* **2019**, *569*, 528. [CrossRef] [PubMed]

175. Somayazulu, M.; Ahart, M.; Mishra, A.K.; Geballe, Z.M.; Baldini, M.; Meng, Y.; Struzhkin, V.V.; Hemley, R.J. Evidence for superconductivity above 260 K in lanthanum superhydride at megabar pressures. *Phys. Rev. Lett.* **2019**, *122*, 027001. [CrossRef] [PubMed]

176. Bickers, N.E.; Scalapino, D.J.; White, S.R. Convserving Approximations for Strongly Correlated Electron Systems: Bethe-Salpeter Equation and Dynamics for the Two-Dimensional Hubbard Model. *Phys. Rev. Lett.* **1989**, *62*, 961. [CrossRef]

177. Pao, C.-H.; Bickers, N.E. Anisotropic superconductivity in the 2D Hubbard model: Gap function and interaction weight. *Phys. Rev. B* **1994**, *49*, 1586. [CrossRef]

178. Monthoux, P.; Scalapino, D.J. Self-consistent $d_x^2 - d_y^2$ pairing in a two-dimensional Hubbard model. *Phys. Rev. Lett.* **1994**, *72*, 1874. [CrossRef]

179. Loram, J.W.; Mirza, K.A.; Cooper, J.R.; Liang, W.Y. Electronic specific heat of $YBa_2Cu_3O_{6+x}$ from 1.8 to 300 K. *Phys. Rev. Lett.* **1993**, *71*, 1740. [CrossRef]

180. Hao, Z.; Clem, J.R.; McElfresh, M.W.; Civale, L.; Malozemoff, A.P.; Holtzberg, F. Model for the reversible magnetization of high-κ type-II superconductors: Application to high-T_c superconductors. *Phys. Rev. B* **1991**, *43*, 2844. [CrossRef] [PubMed]

181. Weber, C.; Haule, K.; Kotliar, G. Critical weights and waterfalls in doped charge-transfer insulators. *Phys. Rev. B* **2008**, *78*, 134519. [CrossRef]

182. Hybertsen, M.S.; Schlüter, M.; Christensen, N.E. Calculation of Coulomb-interaction parameter for La_2CuO_4 using a constrained-density-functional approach. *Phys. Rev. B* **1989**, *39*, 9028. [CrossRef] [PubMed]

183. Eskes, H.; Sawatzky, G.A.; Feiner, L.F. Effective transfer for singlets formed by hole doping in the high-T_c superconductors. *Physica C* **1989**, *160*, 424–430. [CrossRef]

184. McMahan, A.K.; Annett, J.F.; Martin, R.M. Cuprate parameters from numerical Wannier functions. *Phys. Rev. B* **1990**, *42*, 6268. [CrossRef]

185. Eskes, H.; Sawatzky, G. Single-, triple-, or multiplel-band Hubbard models. *Phys. Rev. B* **1991**, *43*, 119. [CrossRef]

186. Otsuka, H. Variational Monte Carlo studies of the Hubbard model in one- and two-dimensions. *J. Phys. Soc. Jpn.* **1992**, *61*, 1645–1656. [CrossRef]

187. Yanagisawa, T.; Koike, S.; Yamaji, K. *d*-wave state with multiplicative correlation factors for the Hubbard model. *J. Phys. Soc. Jpn.* **1999**, *68*, 3608–3614. [CrossRef]

188. Eichenberger, D.; Baeriswyl, D. Superconductivity and antiferromagnetism in the-dimensional Hubbard model: A variational study. *Phys. Rev. B* **2007**, *76*, 180504. [CrossRef]

189. Baeriswyl, D.; Eichenberger, D.; Menteshashvii, M. Variational ground states of the two-dimensional Hubbard model. *New J. Phys.* **2009**, *11*, 075010. [CrossRef]

190. Baeriswyl, D. Superconductivity in the repulsive Hubbard model. *J. Superconduct. Novel Magn.* **2011**, *24*, 1157–1159. [CrossRef]

191. Yanagisawa, T. Quantum Monte Carlo diagonalization for many-fermion systems. *Phys. Rev. B* **2007**, *75*, 224503. [CrossRef]

192. Misawa, T.; Imada, M. Origin of high-T_c superconductivity in doped Hubbard models and their extensions: Roles of uniform charge fluctuations. *Phys. Rev. B* **2014**, *90*, 115137. [CrossRef]

193. Yanagisawa, T.; Miyazaki, M.; Yamaji, K. Crossover induced electron pairing and superconductivity by kinetic renormalization in correlated electron systems. *Condens. Matter* **2018**, *3*, 26. [CrossRef]

194. Kondo, J. *The Physics of Dilute Magnetic Alloys*; Cambridge University Press: Cambridge, UK, 2012.

195. Yanagisawa, T. Kondo effect in the presence of spin-orbit coupling. *J. Phys. Soc. Jpn.* **2012**, *81*, 094713. [CrossRef]

196. Yanagisawa, T. Kondo effect in Dirac systems. *J. Phys. Soc. Jpn.* **2015**, *84*, 074705. [CrossRef]

197. Ellis, R.K.; Stirling, W.J.; Webber, B.R. *QCD and Collider Physics*; Cambridge University Press: Cambridge, UK, 1996.

198. Nozieres, P.; Schmitt-Rink, S. Bose condensation in an attractive fermi gas: From weak to strong coupling superconductivity. *J. Low Temp. Phys.* **1985**, *59*, 195–211. [CrossRef]

199. Rajaraman, R. *Solitons and Instantons*; North-Holland: Amsterdam, The Netherlands, 1989.

200. Solyom, J. The Fermi gas model of one-dimensional conductors. *Adv. Phys.* **1979**, *28*, 201–303. [CrossRef]

201. Yanagisawa, T. Chiral sine-Gordon model. *EPL* **2016**, *113*, 41001. [CrossRef]

202. Yanagisawa, T. Renormalization group analysis of the hyperbolic sine-Gordon model. *Prog. Theor. Exp. Phys.* **2019**, *2019*, 023A01. [CrossRef]

203. Gross, D.; Neveu, A. Dynamical Symmetry breaking in asymptotically free field theories. *Phys. Rev. D* **1974**, *10*, 3235. [CrossRef]